



HAL
open science

A Novel Heat Transfer Coefficient Identification Methodology for the Profile Extrusion Calibration Stage

Filipe Marques, Stéphane Clain, Gaspar Machado, Bruno Martins, Olga Sousa Carneiro, Miguel João Nóbrega

► **To cite this version:**

Filipe Marques, Stéphane Clain, Gaspar Machado, Bruno Martins, Olga Sousa Carneiro, et al.. A Novel Heat Transfer Coefficient Identification Methodology for the Profile Extrusion Calibration Stage. Applied Thermal Engineering, 2016, 103, pp.102-111. 10.1016/j.applthermaleng.2016.04.013 . hal-01251310

HAL Id: hal-01251310

<https://hal.science/hal-01251310>

Submitted on 5 Jan 2016

HAL is a multi-disciplinary open access archive for the deposit and dissemination of scientific research documents, whether they are published or not. The documents may come from teaching and research institutions in France or abroad, or from public or private research centers.

L'archive ouverte pluridisciplinaire **HAL**, est destinée au dépôt et à la diffusion de documents scientifiques de niveau recherche, publiés ou non, émanant des établissements d'enseignement et de recherche français ou étrangers, des laboratoires publics ou privés.



Distributed under a Creative Commons Attribution - NonCommercial 4.0 International License

A Novel Heat Transfer Coefficient Identification Methodology for the Profile Extrusion Calibration Stage

Filipe Marques^a, Stéphane Clain^{a,c}, Gaspar J. Machado^a, Bruno Martins^b, Olga S. Carneiro^b, João M. Nóbrega^b

^a*Centre of Mathematics, University of Minho, Campus de Azurém, 4800-058 Guimarães, Portugal*
e-mail: a62055@alunos.uminho.pt, {clain,gjm}@math.uminho.pt

^b*Institute for Polymers and Composites/I3N, University of Minho, Campus de Azurém, 4800-058*
Guimarães, Portugal

e-mail: brunodiogomartins22@gmail.com, {olgasc,mnobrega}@dep.uminho.pt

^c*Institut de Mathématiques de Toulouse, Université Paul Sabatier, 31062 Toulouse, France*

Abstract

A new method to compute heat transfer coefficients of the profile extrusion process calibration stage, in conjunction with a prototype calibration system [1], is proposed. The methodology involves two major ingredients: a numerical modeling code and a fitting procedure. The code, based on the Finite Volume Method, computes the steady-state solution for the heat transfer problem. The software carefully handles discontinuous solutions as well as discontinuities of the velocity and the material characteristics. Fitting procedure introduces alternative algorithms we have tested and assessed in [2]. A real case study demonstrates the advantages of using the new proposed methodology when compared with the previously applied [1].

Keywords: Profile extrusion cooling stage, heat transfer coefficient identification, fitting, finite volume method, polymer flow

1. Introduction

As in other industrial areas, the numerical simulation of the extrusion process is a fundamental tool to support the design and development of extruders, extrusion dies, and calibration/cooling systems, in order to optimize the production rate while providing high quality products [3, 4]. Basically, in the case of thermoplastics extrusion, the numerical model consists of coupling the Navier-Stokes equations for non-Newtonian material and the non-linear convection-diffusion equation for the thermal process, or the Stefan equation when a phase change occurs. When the extrusion of thermoplastics profile is considered, specific difficulties arise in the numerical simulation of the heat transfer that holds at the calibration/cooling unit. In fact, special attention has to be paid to the interface between the polymer and the calibrator where, due to the non-perfect contact between the two physical domains, a temperature discontinuity exists. Numerical methods such as the finite element [5, 6, 7, 8] or finite difference hardly provide a good approximation of the cooling process since they require continuity across the contact boundary. Moreover, such methods do not guarantee local energy conservation at the

cell level and may lead to unrealistic evaluation of the heat transfer process. The finite volume method is a popular technique due to its built-in conservative property [9]. Its simplicity and versatility turns the method to be very competitive when compared with the traditional finite element method [10, 11, 12] or its recent extension, the finite pointset method [13, 14]. Many practical problems in physics and engineering are now discretized using this robust technique on unstructured meshes, and recent progress enables to consider a wide range of applications for two and three dimensional domains. In particular, the finite volume method easily handles discontinuous solutions or discontinuous material coefficients, while still preserving both the local energy conservation and the accuracy.

Increasing the production rate and the quality of the produced profiles are two antagonistic goals, since the increase of the production speed generally leads to a decrease in the product quality. The cooling stage is critical since it generally determines the production rate, i.e. it is the limiting stage of the extrusion process, and may have a strong influence on the profile quality as it determines the degree of residual stresses present in the final product. The low thermal diffusivity of thermoplastics is the major reason for that behavior. On one hand it slows down the profile cooling process, demanding long residence times in the cooling unit, and, on the other hand it is responsible for the development of huge thermal gradients that give rise to internal residual stresses, thus decreasing the profile performance. Consequently, the cooling stage has a crucial role since solidification of the profile outer layers should be as fast as possible and, at the same time, temperature non-homogeneity should be minimized. To circumvent this problem, the authors of this work have been developing several numerical codes to deal with the heat transfer at the calibration/cooling unit, and concluded that one of the most influential parameters, required as input in the numerical codes, is the heat transfer coefficient at the polymer-calibrator interface, h_{int} . In turn, this coefficient highly depends on process conditions (such as the roughness of the calibration material, the extrusion velocity, and the degree of vacuum, among others) and may vary within a wide range [1]. Therefore, in the simulations of the calibration/cooling stage, accurate values of h_{int} , determined in well controlled conditions, should be considered. For this sake, a prototype calibration/cooling system, previously presented in [1], was developed, being the numerical codes developed for simulation purposes also used to compute, by inverse engineering, h_{int} . However, the determination of this coefficient resorting to the referred prototype faces some other difficulties since an accurate model and numerical scheme are mandatory to provide approximations leading to a correct valuation of this coefficient [15]. In [16], it is shown that the generic second-order finite volume scheme for the convection-diffusion-reaction equation based on the cell to vertex technology is very efficient and robust. In [17] the scheme is tested for non-homogeneous and anisotropic problems.

Furthermore, the determination of h_{int} requires the introduction, as input variables, of some quantities that are not known with enough accuracy. Those variables are the convection heat transfer coefficient of the air, h_{air} , the polymer inflow temperature (i.e. polymer temperature at the extrusion die outlet), T_{in} , and the air temperature, T_{air} (see Fig. 1(a)). Bearing this in mind, to correctly compute the values of the aforementioned parameters during the experimental determination of h_{int} , the temperature of the extruded tape should be measured in several locations. The objective is to minimize the error associated with the h_{int} value, through the use of a function that will opti-

mize, simultaneously, the values of all the unknowns (h_{int} , h_{air} , T_{int} , and T_{air}) in the reverse mode usage of the heat transfer numerical code. It should be noted that the uncertainty of the values of the referred variables (h_{air} , T_{in} , and T_{air}) are expected to have a much higher impact in the determination of h_{int} than in the simulation of the calibration/cooling stage.

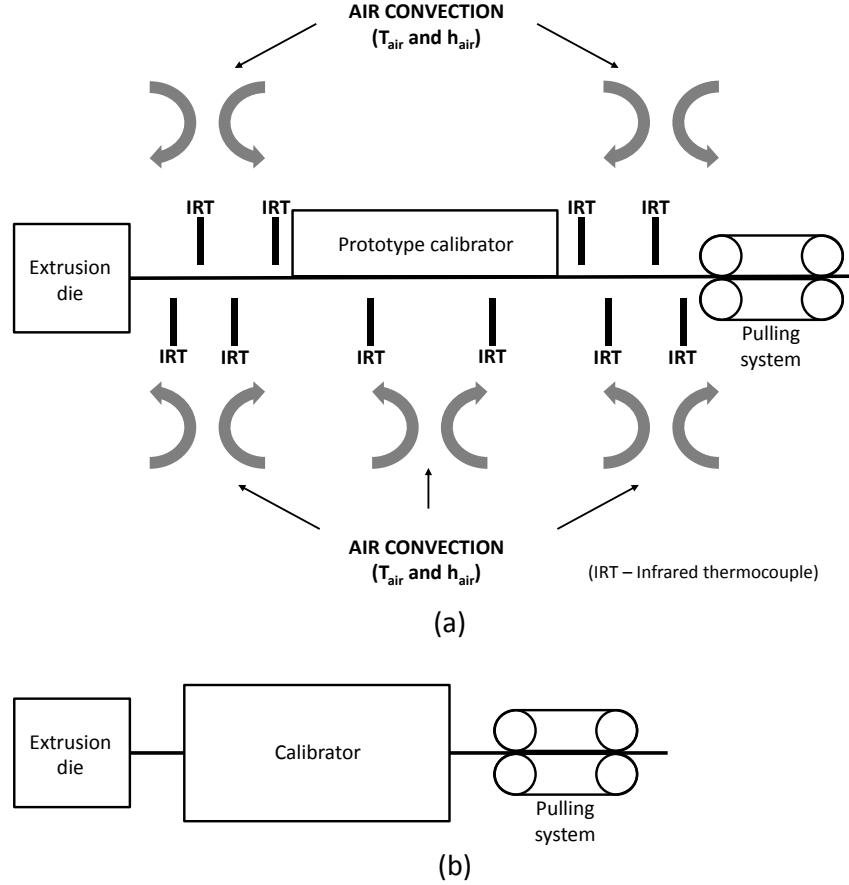


Figure 1: Calibration stage schematic layout:(a) prototype developed to characterize h_{int} ; (b) Typical extrusion line.

In fact, in the prototype calibrator used to determine h_{int} the extruded polymer tape is exposed to environmental conditions during the entire path (both surfaces before and after the prototype, and the lower surface during calibration), as can be seen in Fig. 1(a). Also, the exposed length is higher to enable the placement of several infrared thermocouples for the measurement of its temperature at several locations. In a real calibration unit, environmental conditions will only affect the (short) tape length outside the calibrator, as illustrated in Fig. 1(b). Thus, in this case the majority of the heat transfer occurs inside the calibrator, where the effect of h_{int} is dominant and much more intensive than that of h_{air} . To sum up, in the present work, we aim to develop an algorithm for the

simultaneous optimization of several parameters of the heat transfer in profile extrusion calibration by employing a method for discontinuous situations, both for the solution and the material coefficients. The study considers an aluminium prototype calibrator cooling a polymer (Polystyrene) tape, where we seek for an accurate optimization of the unknown parameters, based on data collected in extrusion runs performed with the referred prototype [1], with a view to determine accurate values for the heat transfer coefficient at the polymer-calibrator interface.

2. The process modelling

As referred in the previous section and illustrated in Fig. 1(b), in a profile extrusion line the polymer profile passes through a calibrator after leaving the extrusion die. The calibrator, as schematized in Fig. 2, is a metallic tool maintained at a low temperature via the circulation of a cold fluid in its cooling channels. It encompasses also several slots through which vacuum is applied to assure the contact between the hot polymer profile and the cold calibration surface. The heat transfer process occurs essentially in the path through the calibrator, and also (at a minor extent) in the air path before and after the calibrator.

In the scope of this work, we consider the multi-domain polymer-calibrator system, represented in Fig. 3 and constituted of two subdomains where Ω_c and Ω_p stand for the calibrator and polymer (the subscripts c and p refer to the calibrator and polymer, respectively) while the boundaries are defined as:

- calibrator: $\Gamma_c = \Gamma_{\text{sup}} \cup \Gamma_{\text{lat}} \cup \Lambda$,
- polymer: $\Gamma_p = \Gamma_{\text{air}} \cup \Gamma_{\text{in}} \cup \Gamma_{\text{out}} \cup \Lambda$.

2.1. Heat transfer problem

A two-dimensional convection-diffusion model based on the energy conservation equations for the two domains is used to model the flow and the extruder, namely

$$\begin{aligned} \nabla \cdot (C_p U_p T_p - k_p \nabla T_p) &= 0 & \text{in } \Omega_p, \\ -\nabla \cdot (k_c \nabla T_c) &= 0 & \text{in } \Omega_c, \end{aligned}$$

where k_p and k_c are the thermal conductivity of the polymer and the calibrator respectively, T_p and T_c represent the temperature distribution in the polymer and the calibrator respectively, and U_p and C_p are the velocity and the volumetric heat capacity of the polymer respectively. We then prescribe the following boundary conditions.

- The heat transfer between the polymer and the calibrator is defined as a thermal contact resistance, which originates a discontinuity in the temperature domain. The energy flux across the interface is assumed to be linear with respect to the difference of the temperatures given by

$$k_c \frac{\partial T_c}{\partial n_c} = -k_p \frac{\partial T_p}{\partial n_p} = h_{\text{int}}(T_p - T_c) \quad \text{on } \Lambda,$$

where n_p and n_c denote the unit normal vector to the boundaries of Ω_p and Ω_c respectively.

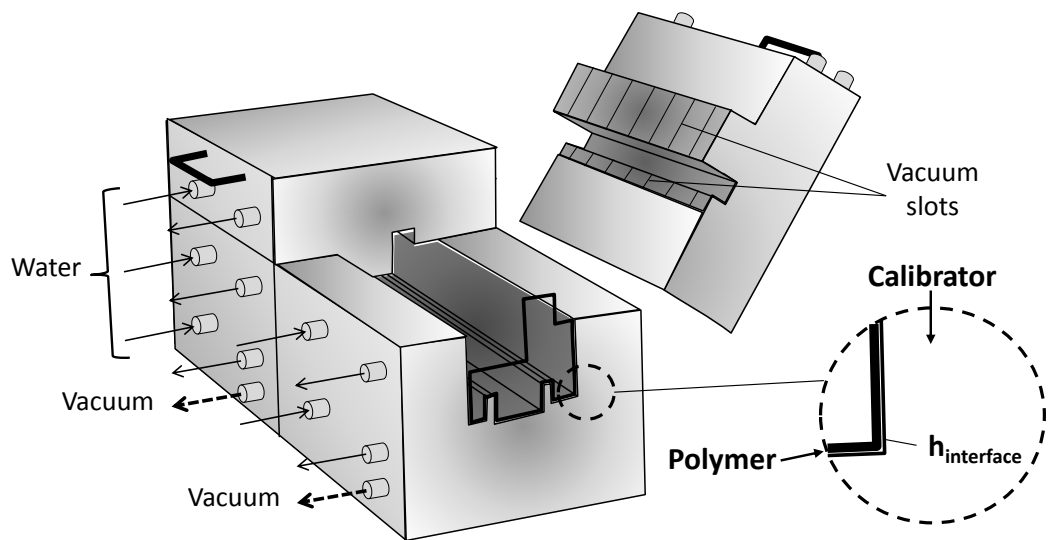


Figure 2: Typical calibration unit for profiles.

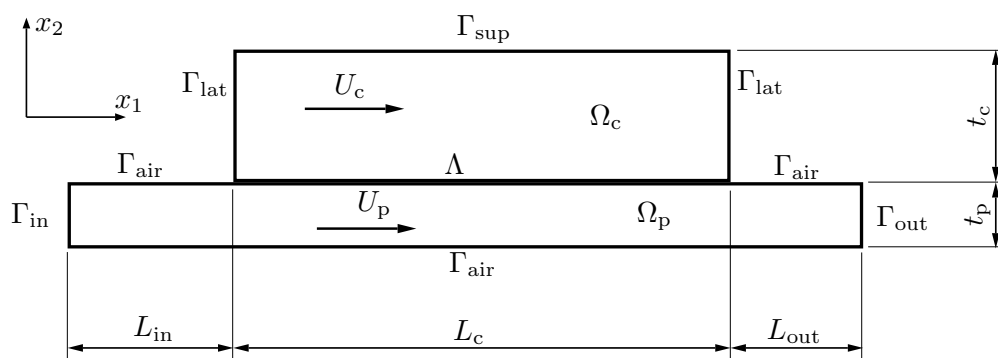


Figure 3: Two-dimensional geometry used to model the heat transfer between the calibrator and the polymer.

- The temperature distribution on Γ_{sup} is a given polynomial function $T_{\text{sup}} = T(x_1)$, experimentally determined with the data provided by thermocouples embedded in the calibrator block [1].
- On the lateral sides of the calibrator, the bottom and the upper surfaces, natural convection is assumed

$$-k_c \frac{\partial T_c}{\partial n_c} = h_{\text{air}}(T_c - T_{\text{air}}) \quad \text{on } \Gamma_{\text{lat}} \cup \Gamma_{\text{air}},$$

where T_{air} denotes the temperature of the air which is considered a constant value, and h_{air} is the natural convection heat transfer coefficient.

- For the polymer inflow left boundary, we assume a constant prescribed temperature $T = T_{\text{in}}$ on Γ_{in} which corresponds to the extrusion temperature, whereas we assume an adiabatic condition for the polymer outflow on the right boundary

$$-k_p \frac{\partial T_p}{\partial n_p} = 0 \quad \text{on } \Gamma_{\text{out}}.$$

3. Finite volume scheme

We provide a short description of the finite volume scheme based on the cell-to-vertex technology presented in [16], that closely follows the scheme proposed in [2]. We consider the energy equation on an open bounded polygonal domain Ω of \mathbb{R}^2 with boundary Γ (we skip the index p for the sake of simplicity). We seek the temperature distribution $T \equiv T(x_1, x_2)$ as a solution of the steady-state convection-diffusion equation

$$\nabla \cdot (VT - k\nabla T) = 0 \quad \text{in } \Omega, \tag{1}$$

where VT is the convective term with $V = CU$ and $k\nabla T$ is the diffusive term. The boundary of the domain is partitioned into four subsets Γ_{D} , Γ_{N} , Γ_{R} , and Λ where different types of conditions may be prescribed, namely:

- Dirichlet: $T = T_{\text{D}}$ on Γ_{D} ;
- Neumann (adiabatic): $-k\nabla T \cdot n = 0$ on Γ_{N} ;
- interface polymer-air: $(VT - k\nabla T) \cdot n = h(T - T_{\text{air}})$ on Γ_{R} .
- interface polymer-calibrator: $k_c \nabla T_c \cdot n_c = -k_p \nabla T_p \cdot n_p = h(T_p - T_c)$ on Λ .

3.1. Mesh and notations

We denote by \mathcal{T} a mesh consisting of I non-overlapping convex polygonal cells c_i , $i = 1, \dots, I$, and K vertices v_k , $k = 1, \dots, K$. We highlight that \mathcal{T} composes two sub-meshes, \mathcal{T}_c and \mathcal{T}_p , for the subdomains Ω_c and Ω_p , respectively, and are conformed with Λ such that if $\hat{e} \cap \Lambda \neq \emptyset$ then $e \subset \Lambda$. We adopt the following conventions (see Fig. 4):

- the mesh \mathcal{T}_c consists of I_c non-overlapping convex polygonal cells c_{i_c} , $i_c = 1, \dots, I_c$, and K_c vertices v_{k_c} , $k_c = 1, \dots, K_c$;

- the mesh \mathcal{T}_p consists of I_p non-overlapping convex polygonal cells c_i , $i_p = I_c + 1, \dots, I_c + I_p$, and K_p vertices v_{k_p} , $k_p = K_c + 1, \dots, K_c + K_p$;
- for any cell c_i , ∂c_i represents its boundary and $|c_i|$ its area; we denote by m_i the mass centre of c_i ;
- two cells c_i and c_j share a common edge e_{ij} whose length is $|e_{ij}|$ and the midpoint is m_{ij} ; n_{ij} is the unit normal vector to e_{ij} outward to c_i , *i.e.* $n_{ij} = -n_{ji}$; if an edge of c_i belongs to the boundary Γ , we replace the index j by D, N, R, or Λ if e_{ij} belongs to Γ_D , Γ_N , Γ_R , or Λ , respectively;
- for any cell c_i belonging to Ω_c or Ω_p we associate the index set $\nu(i_c) \subset \{1, \dots, I_c\} \cup \{D, N, R, \Lambda\}$ or $\nu(i_p) \subset \{I_c + 1, \dots, I_c + I_p\} \cup \{D, N, R, \Lambda\}$, respectively, such that $j \in \nu(i)$ if e_{ij} is a common edge of c_i and c_j or with the boundary Γ_j if $j = \{D, N, R\}$ or with the interface Λ ;
- for any vertex v_k belonging to Ω_c or Ω_p we associate the index set $\mu(k_c) \subset \{1, \dots, I_c\}$ or $\mu(k_p) \subset \{I_c + 1, \dots, I_c + I_p\}$, respectively, such that $i \in \mu(k)$ if v_k is a vertex belonging to the cell c_i .

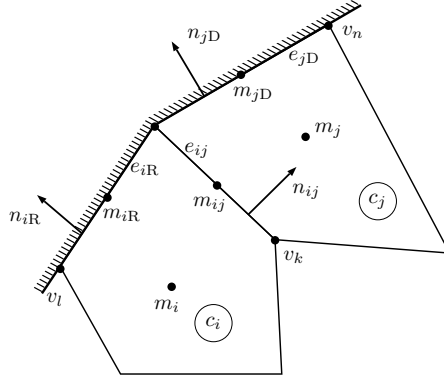


Figure 4: Mesh notation.

3.2. Second-order scheme

To provide the finite volume scheme, Eq. (1) should be integrated over cell c_i

$$\int_{c_i} \nabla \cdot (VT - k\nabla T) dx = 0,$$

and applying the divergence theorem we get an integral over the surface

$$\int_{\partial c_i} (VT - k\nabla T) \cdot n ds = 0,$$

and, then,

$$\sum_{j \in \nu(i)} \int_{e_{ij}} (V \cdot n_{ij} T - k \nabla T \cdot n_{ij}) ds = 0. \quad (2)$$

The numerical integration of Eq. (2), based on a quadrature method, introduces consistency second-order errors and provides the following approximation

$$\sum_{j \in \nu(i)} |e_{ij}| (V(m_{ij}) \cdot n_{ij} T(m_{ij}) - k(m_{ij}) \nabla T(m_{ij}) \cdot n_{ij}) \approx 0. \quad (3)$$

The residual is a function of the vector \mathbf{T} given by

$$\mathcal{G}_i(\mathbf{T}) = \sum_{j \in \nu(i)} |e_{ij}| \mathcal{F}_{ij}(\mathbf{T})$$

where \mathcal{F}_{ij} is an approximation of the convective and diffusive fluxes through the edge e_{ij} presented in Eq. (3).

3.3. Flux computation

Cell centred finite volume methods use the cell centre as collocation points for the unknowns. Nevertheless, the computation of the gradients require an evaluation of the temperature at the vertices. The cell-to-vertex interpolation provides a robust and accurate mechanism to compute the temperature at vertices from the temperature at the cell centres. Let T_i be an approximation of T at m_i . We gather all the approximations in two vectors $\mathbf{T}_c = (T_i)_{i=1, \dots, I_c}$ and $\mathbf{T}_p = (T_i)_{i=I_c+1, \dots, I_c+I_p}$ for the calibrator and the polymer domain. Similarly, let $\Theta_c = (\theta_{k_c})_{k_c=1, \dots, K_c}$ and $\Theta_p = (\theta_{k_p})_{k_p=K_c+1, \dots, K_c+K_p}$ be the vectors with the approximations of the temperature at the vertices. We also consider the global vectors $\mathbf{T} = (\mathbf{T}_c, \mathbf{T}_p)^t$ and $\Theta = (\Theta_c, \Theta_p)^t$ corresponding to the temperature distribution in the whole domain associated to the cells and to the vertices respectively.

The linear mapping $\mathbf{T} \rightarrow \Theta(\mathbf{T})$ given by

$$\theta_k = \sum_{i \in \mu(k)} \beta_{ki} T_i$$

with β_{ki} the interpolation coefficients for vertex k provides an expression of the temperature at the vertex v_i in function of the temperature in the cell c_i , $i \in \mu(k)$. Special attention is required when dealing with the discontinuity at the contact interface and two distinct temperatures have to be evaluated at the same vertex (see [2] for a detailed description of the method). The numerical fluxes are then evaluated based on the two vectors \mathbf{T} and Θ .

- For each cell c_i we define the affine function

$$\tilde{T}_i(x_1, x_2) = T_i + \tilde{\mathcal{C}}_{i,1}(x_1 - m_{i,1}) + \tilde{\mathcal{C}}_{i,2}(x_2 - m_{i,2}),$$

where $\tilde{\mathcal{C}}_{i,1}$ and $\tilde{\mathcal{C}}_{i,2}$ are the coefficients that minimize a quadratic functional and correspond to the best approximation in the least squares sense of the temperature θ_k at the vertices of the cell.

- Each inner edge holds two different polynomials \tilde{T}_{ij} and \tilde{T}_{ji} given by

$$\tilde{T}_{ij}(x_1, x_2) = T_i + \tilde{\mathcal{C}}_{ij,1}(x_1 - m_{i,1}) + \tilde{\mathcal{C}}_{ij,2}(x_2 - m_{i,2}),$$

and the symmetric expression for \tilde{T}_{ji} , where $\tilde{C}_{ij,1}$ and $\tilde{C}_{ij,2}$ are the unique coefficients that the resultant polynomial interpolates θ_k , associated to the two extremities v_k of e_{ij} . The polynomial associated to edge e_{ij} then writes

$$\tilde{T}_{ij} = \tilde{T}_{ji} = \frac{|c_i|}{|c_i| + |c_j|} \tilde{T}_{ij} + \frac{|c_j|}{|c_i| + |c_j|} \tilde{T}_{ji}.$$

Denoting $[z]^+ = \max(0, z)$ and $[z]^- = \min(0, z)$, the numerical fluxes should take into account four different situations:

- for an inner edge e_{ij} as

$$\mathcal{F}_{ij} = [V(m_{ij}) \cdot n_{ij}]^+ \tilde{T}_i(m_{ij}) + [V(m_{ij}) \cdot n_{ij}]^- \tilde{T}_j(m_{ij}) - k(m_{ij}) \nabla \tilde{T}_{ij}(m_{ij}) \cdot n_{ij};$$

- for a Dirichlet boundary edge e_{iD} as

$$\mathcal{F}_{iD} = [V(m_{iD}) \cdot n_{iD}]^+ \tilde{T}_i(m_{iD}) + [V(m_{iD}) \cdot n_{iD}]^- T_D(m_{iD}) - k(m_{iD}) \nabla \tilde{T}_{iD}(m_{iD}) \cdot n_{iD};$$

- for a Neumann boundary edge e_{iN} as

$$\mathcal{F}_{iN} = V(m_{iN}) \cdot n_{iN} \tilde{T}_i(m_{iN});$$

- for a heat transfer boundary edge e_{iR} as

$$\mathcal{F}_{iR} = h \left(\tilde{T}_i(m_{iR}) - T_R(m_{iR}) \right).$$

In the case of the interface between the polymer and the calibrator, we have to distinguish two cases regarding to the side where the flux comes from (see [2] for the details).

Since \mathcal{F}_{ij} is linearly dependent on vector \mathbf{T} , we define the affine operator $\mathbf{T} \rightarrow \mathcal{G}_i(\mathbf{T})$ for each cell c_i , $i = 1, \dots, I$. Gathering all the components $\mathcal{G}_i(\mathbf{T})$ of the residual in vector $\mathcal{G}(\mathbf{T})$, we seek the solution vector \mathbf{T}^* such that $\mathcal{G}(\mathbf{T}^*) = 0_I$. We obtain a matrix-free scheme and the affine problem is solved by applying a preconditioned GMRES procedure.

4. Parameter identification procedure

We assume that the cooling process is mainly governed by five parameters: the heat transfer coefficients h_{int} and h_{air} , the temperatures T_{air} and T_{in} , and the velocity u . In practice, some coefficients are measured (temperature, velocity) while the other parameters have to be deduced from the experimental tests. To this end, several sensors measure the temperature \hat{T}_{p_ℓ} at points q_ℓ , $\ell = 1, \dots, C_\ell$, and the goal is to identify the set of parameters

$$\mathbf{H} = (H_1, \dots, H_m)$$

that provides the polymer temperature approximation $T_p^{\mathbf{H}}$ that better suits the experimental measurements. More precisely, we seek the set of m parameters \mathbf{H} that minimize

the error between the measured temperatures and its the numerical approximation given by the following functional

$$F(\mathbf{H}) = \sum_{\ell=1}^{C_\ell} \left[T_p^{\mathbf{H}}(q_\ell) - \hat{T}_{p_\ell} \right]^2, \quad (4)$$

where C_ℓ is the number of sensors.

Notice that the set of parameters \mathbf{H} may be different from an operation to another one in function of the experimental conditions. Indeed, one can consider a problem with two parameters as $\mathbf{H} = (h_{\text{int}}, h_{\text{air}})$ if the others parameters are given or a problem with four parameters as $\mathbf{H} = (h_{\text{int}}, h_{\text{air}}, T_{\text{air}}, T_{\text{in}})$ when the temperatures also are unknown.

To provide the optimal set of parameters, an iterative procedure is considered where a variation $\Delta\mathbf{H}^n$ to the parameters \mathbf{H}^n provides a better approximation $\mathbf{H}^{n+1} = \mathbf{H}^n + \Delta\mathbf{H}^n$ such that $F(\mathbf{H}^{n+1}) < F(\mathbf{H}^n)$. Several optimization techniques will be considered to achieve this goal.

4.1. The Newton-Raphson method

The Newton-Raphson technique is a generic procedure to provide the zeros of a vector-valued function using successive linear approximations. Since we want to minimize function F , we seek vector \mathbf{H} such that $\nabla F(\mathbf{H}) = \mathbf{0}$. We then introduce

$$\Delta\mathbf{H} = - [\nabla^2 F(\mathbf{H})]^{-1} \nabla F(\mathbf{H}),$$

where ∇F is the gradient vector and $\nabla^2 F$ denotes the Hessian matrix.

To evaluate the derivatives, the finite differences were adopted. We define a tolerance value ε and set

$$\varepsilon_\alpha = H_\alpha \varepsilon, \quad \alpha = 1, \dots, m.$$

An approximation of the first derivatives then writes

$$\frac{\partial F}{\partial H_i} \approx \frac{F(H_i + \varepsilon_i, \dots) - F(H_i - \varepsilon_i, \dots)}{2\varepsilon_i}$$

and we proceed in a similar way to evaluate approximations for the second derivative $\frac{\partial^2 F}{\partial H_i \partial H_j}$ involved in the Hessian matrix.

Notice that the optimization procedure requires to evaluate $1 + 2m^2$ times the function F in each iteration, which means that the thermal problem has to be solved the same amount of times leading to an important and unnecessary computational effort.

4.2. The Gauss-Newton method

The Gauss-Newton method is a specific modification of the Newton-Raphson method for nonlinear least squares problems. The main advantage is that much less computational effort is required since it avoids the calculation of second derivatives.

The least squares problem given by Eq. (4) can be rewritten in vectorial form as

$$F(\mathbf{H}) = \left(\mathbf{T}_p^{\mathbf{H}} - \hat{\mathbf{T}}_p \right)^T \left(\mathbf{T}_p^{\mathbf{H}} - \hat{\mathbf{T}}_p \right). \quad (5)$$

In order to evaluate the temperature distribution in the neighborhood of \mathbf{H} , we consider the first-order Taylor series expansion, yielding

$$\mathbf{T}_p^{\mathbf{H}+\Delta\mathbf{H}} \approx \mathbf{T}_p^{\mathbf{H}} + \frac{\partial \mathbf{T}_p^{\mathbf{H}}}{\partial \mathbf{H}} \Delta\mathbf{H} = \mathbf{T}_p^{\mathbf{H}} + \mathbf{J} \Delta\mathbf{H}, \quad (6)$$

where $\frac{\partial \mathbf{T}_p^{\mathbf{H}}}{\partial \mathbf{H}}$ is the Jacobian matrix, and it will be denoted by \mathbf{J} . Considering Eq. (6) in Eq. (5), we can estimate the error for a perturbation of the parameters

$$\begin{aligned} F(\mathbf{H} + \Delta\mathbf{H}) &\approx \left(\mathbf{T}_p^{\mathbf{H}} + \mathbf{J} \Delta\mathbf{H} - \hat{\mathbf{T}}_p \right)^T \left(\mathbf{T}_p^{\mathbf{H}} + \mathbf{J} \Delta\mathbf{H} - \hat{\mathbf{T}}_p \right) \\ &= F(\mathbf{H}) - 2(\mathbf{J} \Delta\mathbf{H})^T \left(\hat{\mathbf{T}}_p - \mathbf{T}_p^{\mathbf{H}} \right) + (\mathbf{J} \Delta\mathbf{H})^T \mathbf{J} \Delta\mathbf{H} \\ &= F(\mathbf{H}) - \Delta\mathbf{H}^T \left[2\mathbf{J}^T \left(\hat{\mathbf{T}}_p - \mathbf{T}_p^{\mathbf{H}} \right) - \mathbf{J}^T \mathbf{J} \Delta\mathbf{H} \right]. \end{aligned}$$

Thus, by identification, we deduce

$$\frac{\partial F}{\partial \Delta\mathbf{H}}(\mathbf{H}) \approx -2\mathbf{J}^T \left(\hat{\mathbf{T}}_p - \mathbf{T}_p^{\mathbf{H}} \right) + \mathbf{J}^T \mathbf{J} \Delta\mathbf{H}. \quad (7)$$

We seek a perturbation $\Delta\mathbf{H}$ that minimizes F , *i.e.* $\frac{\partial F}{\partial \Delta\mathbf{H}} = \mathbf{0}$. Therefore Eq. (7) provides the expression

$$\Delta\mathbf{H} = [\mathbf{J}^T \mathbf{J}]^{-1} \mathbf{J}^T \left(\hat{\mathbf{T}}_p - \mathbf{T}_p^{\mathbf{H}} \right). \quad (8)$$

Notice that calculation of $\Delta\mathbf{H}$ only requires the Jacobian matrix and the Gauss-Newton method is less computational consuming when compared with Newton-Raphson technique, since for each iteration the thermal problem has to be solved $1 + m$ times.

4.3. The Levenberg-Marquardt method

The Levenberg-Marquardt method is also a specific technique to solve nonlinear least squares problems where the parameters variation is an interpolation between the Gauss-Newton method and the gradient descent method. Levenberg replaced Eq. (8) by a damped version given as [18]

$$\Delta\mathbf{H} = [\mathbf{J}^T \mathbf{J} + \lambda \mathbf{I}]^{-1} \mathbf{J}^T \left(\hat{\mathbf{T}}_p - \mathbf{T}_p^{\mathbf{H}} \right), \quad (9)$$

where λ is a non-negative damping factor and \mathbf{I} denotes the identity matrix. This factor provides a better stability and increases the admissible convergence basin where one can choose the initial condition. Notice that we recover the Gauss-Newton method with $\lambda = 0$. The critical point consists in choosing the damping factor since too large values will reduce the efficiency of the method and dramatically increase the computational cost. Heuristic approaches to evaluate the the factor have been given in [18]

To avoid slow convergence in the direction of small gradients, Marquardt [19] proposed to scale the components of the gradient substituting the identity matrix by a diagonal matrix with the elements of the diagonal of $\mathbf{J}^T \mathbf{J}$, and Eq. (9) becomes

$$\Delta\mathbf{H} = [\mathbf{J}^T \mathbf{J} + \lambda \text{diag}(\mathbf{J}^T \mathbf{J})]^{-1} \mathbf{J}^T \left(\hat{\mathbf{T}}_p - \mathbf{T}_p^{\mathbf{H}} \right). \quad (10)$$

There are several versions for the Levenberg-Marquardt method. The difference between them relies on the criterion for the convergence evaluation and on the evolution of the parameter λ . For this work, we accept the results of an iteration n if the parameter ρ^n is larger than a given tolerance ϵ [20]. Hence,

$$\rho^n = \frac{F(\mathbf{H}) - F(\mathbf{H} + \Delta\mathbf{H})}{2\Delta\mathbf{H}^T \left(\lambda^n \Delta\mathbf{H} + \mathbf{J}^T \left(\hat{\mathbf{T}}_p - \mathbf{T}_p^{\mathbf{H}} \right) \right)}.$$

To start this process a initial value for the damping factor λ_0 should be provide by the user. If the previous criterion is satisfied, the perturbation $\Delta\mathbf{H}$ is accepted and λ is reduced till a limit value

$$\lambda^{n+1} = \max \left[\frac{\lambda^n}{L_{\text{dn}}}; \lambda_{\text{min}} \right].$$

Otherwise the set of parameters \mathbf{H} remains unaltered, and λ is increased

$$\lambda^{n+1} = \min [\lambda^n L_{\text{up}}; \lambda_{\text{max}}].$$

The evaluation of the terms of Eq. (10) follows the same procedure as Gauss-Newton method. Thus, the Levenberg-Marquardt method also need to solve the thermal problem $1 + m$ times in each iteration.

5. Synthetic tests

We propose several synthetic benchmarks to assess the efficiency and robustness of the minimization methods. A set of parameter of reference is chosen to compute the reference solution. We then select 10 points on the upper and lower surfaces of the polymer we shall use in the identification algorithm. The first benchmark aims to compare the three minimization methods in terms of convergence and computational cost where we show that the Gauss-Newton method is the best compromise. The second benchmark deals with the basin of convergence. Random initial parameters are prescribed and we assess the method ability to recover the reference parameters.

5.1. The manufactured reference solution

To design the manufactured solution, we use $L_{\text{in}} = 0.17\text{m}$, $L_{\text{c}} = 0.3\text{m}$, $L_{\text{out}} = 0.13\text{m}$, $t_{\text{p}} = 1.42 \times 10^{-3}\text{m}$, and $t_{\text{c}} = 0.012\text{m}$. The material properties are $k_{\text{p}} = 0.17\text{W}/(\text{m K})$, $k_{\text{c}} = 123\text{W}/(\text{m K})$, $\rho_{\text{p}} = 1040\text{kg}/\text{m}^3$, and $c_{p_{\text{p}}} = 2050\text{J}/(\text{kg K})$. The extrusion velocity is $0.0175\text{m}/\text{s}$, and the temperature on Γ_{sup} is approximated by a polynomial function, based on the values measured by a set of thermocouples, which is given as

$$T_{\text{sup}} = 48180x_1^5 - 45151x_1^4 + 15502x_1^3 - 2366.9x_1^2 + 142.77x_1 + 308.4, \quad x_1 \in [0; 0.3].$$

For the remaining boundary conditions, it was defined $h_{\text{int}} = 500\text{W}/(\text{m}^2\text{K})$, $h_{\text{air}} = 50\text{W}/(\text{m}^2\text{K})$, $T_{\text{in}} = 493\text{K}$ (220°C), and $T_{\text{air}} = 298.5\text{K}$ (25.5°C).

As the set calibrator/polymer has a regular geometry, we use a structured quadrangular mesh as displayed in Fig. 5 where N_{p} , N_{c} , and N_{h} denote the number of elements on polymer and calibrator on x_2 direction and the number of elements on x_1 direction on calibrator, respectively.

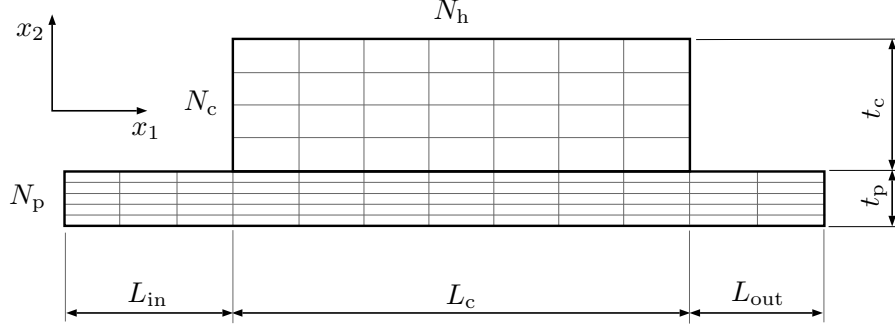


Figure 5: Schematic mesh for the polymer/calibrator model.

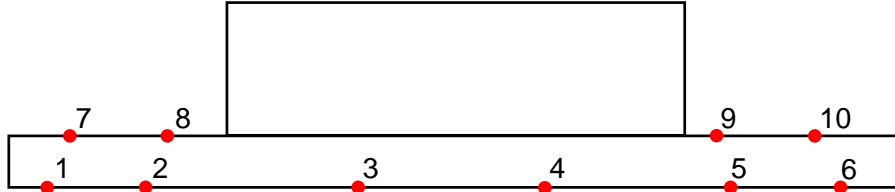


Figure 6: Representation of the measured points location.

Table 1: Coordinates and temperatures obtained numerically in the considered points.

point	coordinate x_1 [m]	coordinate x_2 [m]	temperature [K]
1	0.045	0.0	466.6869
2	0.081	0.0	456.1800
3	0.221	0.0	418.5102
4	0.395	0.0	355.3805
5	0.471	0.0	339.6116
6	0.587	0.0	327.1214
7	0.103	1.42×10^{-3}	450.1617
8	0.137	1.42×10^{-3}	441.3151
9	0.485	1.42×10^{-3}	326.0922
10	0.527	1.42×10^{-3}	328.0068

The thermal model was evaluated with the given parameters and the temperature data was extracted at the 10 points given in Fig. 6 and reported in Table 1 (coordinates and temperatures). We define the dimensionless error estimator

$$E_n = \sum_i \frac{2(H_i^{n+1} - H_i^n)}{H_i^{n+1} + H_i^n}$$

and we stop the iterative procedure when the error between two consecutive iterations is lower than 1×10^{-4} .

5.2. Minimization methods comparison

Convergence tests for the Newton-Raphson method, the Gauss-Newton method, and the Levenberg-Marquardt method are carried out to select the most performavit algorithm. For this benchmark, a set of four parameters is considered, namely: the heat transfer coefficient at the polymer/calibrator interface, the convection heat transfer coefficient of the air, the polymer inflow temperature, and the temperature of the air.

We proceed in the following way: all the parameters are set to the reference values except one that we set to 90% of the reference value. Computation is then carried out and we evaluate the number of iterations to reach the reference values. We then obtain four numerical tests where we successively perturb h_{int} , h_{air} , T_{in} , and T_{air} . In Fig. 7 it is displayed the dimensionless error curves for the Newton-Raphson method. We notice that the method did not converge for the cases where h_{air} and T_{air} were perturbed, which disqualify the algorithm for future applications.

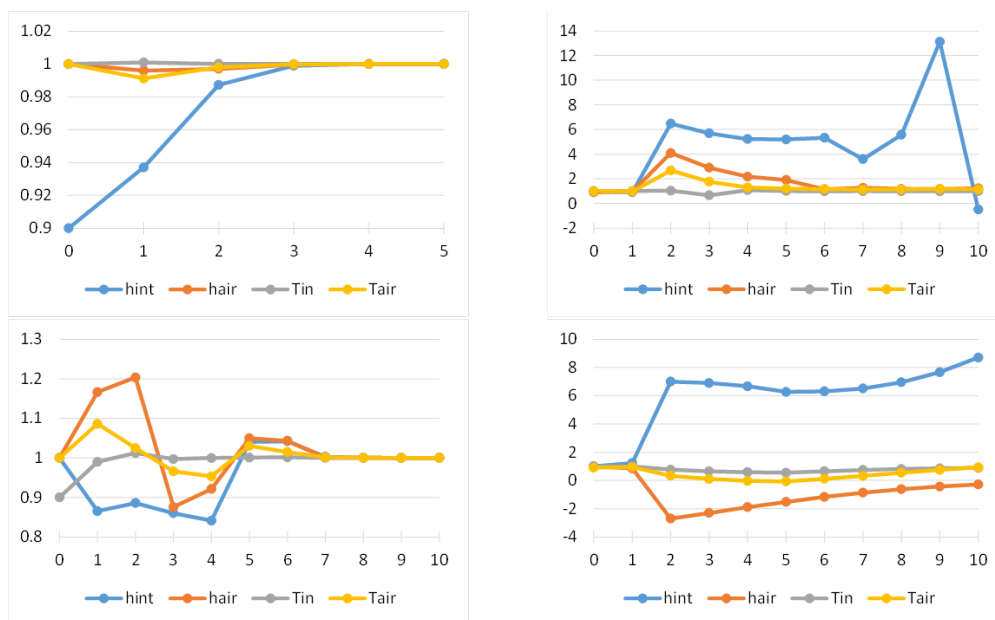


Figure 7: The evolution of the parameters during the optimization with Newton-Raphson with initial variations of h_{int} (top left), h_{air} (top right), T_{in} (down left), and T_{air} (down right).

We proceed in the same way with the Gauss-Newton technique and we report in Fig. 8 the error curves with respect to the number of iterations. Convergence is achieved in all the situations which qualifies the method to be used in more complex situations.

At last, the Levenberg-Marquardt method is tested for the same situations. The additional parameters required by the method are $\epsilon = 1 \times 10^{-2}$, $\lambda_{\text{min}} = 1 \times 10^{-7}$, $\lambda_{\text{max}} = 1 \times 10^7$, $L_{\text{dn}} = 9$, and $L_{\text{up}} = 11$. It is given in Fig. 9 the error curves for the four perturbations and observe that the algorithm converged in all the cases.

We report in Table 2 the number of iterations and time consuming (in seconds) for each test. The Newton-Raphson technique is clearly the worst algorithm whereas the Gauss-Newton and Levenberg-Marquardt methods are faster and converged in all tests.

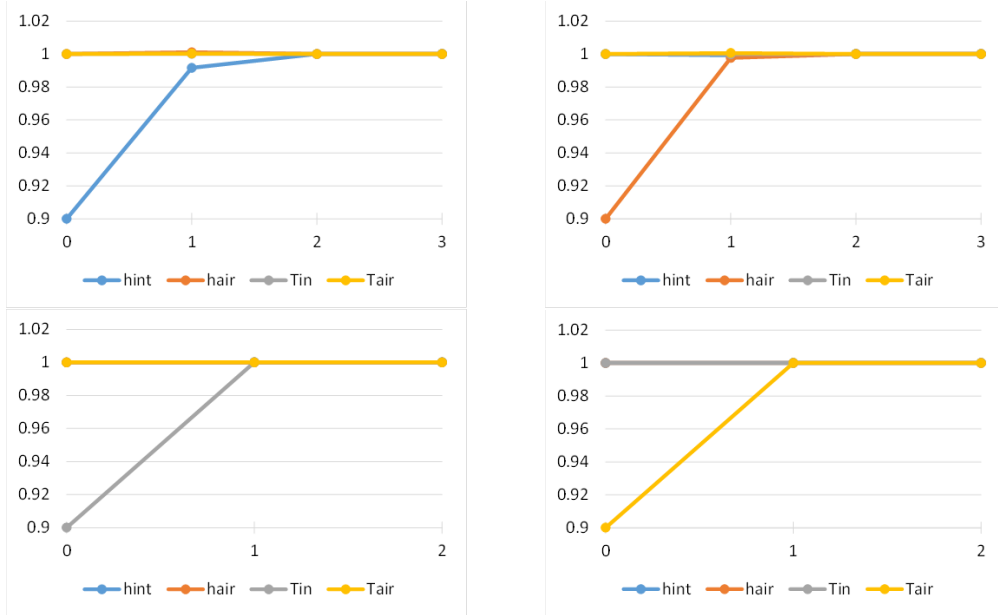


Figure 8: The evolution of the parameter during the optimization with Gauss-Newton with initial variations of h_{int} (top left), h_{air} (top right), T_{in} (down left), and T_{air} (down right).

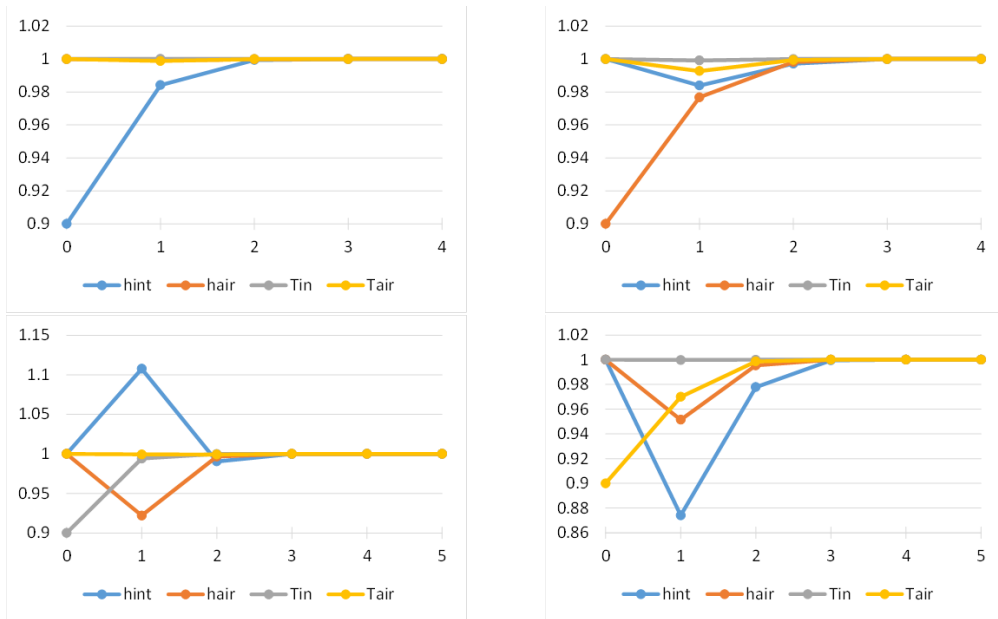


Figure 9: The evolution of the parameter during the optimization with Levenberg-Marquardt with initial variations of h_{int} (top left), h_{air} (top right), T_{in} (down left), and T_{air} (down right).

On the other hand, the Gauss-Newton method is more efficient with less iterations to converge for the correct solution. So, we will adopt the Gauss-Newton algorithm to carry out all the following benchmarks and tests.

Table 2: Summary of the presented tests.

	h_{int}		h_{air}		T_{in}		T_{air}		all	
	iter	time	iter	time	iter	time	iter	time	iter	time
NR	5	1714.1	—	—	10	3514.3	—	—	5	1581.25
GN	3	142.89	3	129.62	2	88.409	2	86.018	4	169.63
LM	4	177.11	4	170.02	5	246.11	5	259.58	5	250.36

5.3. Test with a control parameter

Beyond the parameters studied in the previous tests, the extrusion velocity will also be included in the identification process. Although this parameter is well defined during the experimental activity, it is used as a control parameter to validate the results. Indeed, since the parameters identification algorithm provides an approximation of the velocity that we compare with the measured (or prescribed) one, we obtain an estimate of the approximation accuracy. Consequently, the velocity has not the status of a unknown parameter but acts as a control parameter which assess the solution quality.

In order to evaluate the basin of convergence, *i. e.* the domain where we can choose the initial condition which guarantees the convergence of the iterative sequence, we choose the initial guess in an interval of $\pm 50\%$ of the reference parameter for h_{int} , h_{air} , and u , and the temperatures (in Kelvin) ranges in a $\pm 10\%$ interval around the reference temperatures. Therefore, the dimensionless value of each parameters for initial approximation can vary between 0.5 and 1.5 or 0.9 and 1.1. Ten random sets of parameters belonging to the admissible initial domain have been chosen (*cf.* Table 3). The additional information shows whether the control parameter coincides with the reference one or not. Only one negative case is reported and we underline that convergence is achieved with at most 5 iterations.

Table 3: Initial approximations for the performed tests and numbers of iterations to reach convergence.

test	1	2	3	4	5	6	7	8	9	10
h_{int}	0.635	0.936	1.156	1.273	0.732	0.805	1.330	1.127	0.609	0.963
h_{air}	1.205	1.464	0.879	1.403	1.143	1.223	1.047	0.872	0.900	1.185
T_{in}	0.954	1.065	0.987	0.932	1.019	0.984	0.967	1.087	0.957	0.969
T_{air}	0.918	1.059	1.079	1.028	0.969	1.008	0.937	1.043	0.996	0.905
u	1.221	1.354	1.256	0.828	0.622	0.643	1.436	1.050	1.201	0.563
convergence	yes (5)	yes (4)	yes (5)	yes (6)	yes (5)	yes (5)	yes (5)	yes (4)	yes (5)	no

6. Experimental case study

The procedures proposed in this work, to find the optimal parameters that meet the experimental data, are now tested in a real situation, with data obtained with the

prototype system, conceived to measure the heat transfer coefficient at the polymer-calibrator interface [1]. For that purpose the prototype system was operated under specific process conditions and the average temperature at several points, identified in Fig. 6, was registered after achieving steady state conditions, during a measurement period of 20 min. Regarding the fitting approach, in all tests performed in this section the Gauss-Newton method was considered, since it was the one that showed the best performance on the previous studies, described in the previous section.

The location of the measured points as well as the system properties, closely follows the data used in the synthetic tests (*cf.* Table 1). During the experiments the air temperature was measured, $T_{\text{air}}=293$ K, and the profile velocity $u=0.0175$ m/s was imposed. Table 4 contains the average temperature values for all points, collected during the experimental run.

Table 4: Temperatures obtained on the experimental test.

point	temperature [K]
1	477.31
2	468.87
3	441.81
4	362.40
5	342.02
6	331.14
7	463.98
8	455.32
9	329.97
10	331.29

The first parameter fitting test (2+2 points) followed the procedure proposed in [1], which consists of using the temperature of points 7 and 8 (see Fig. 6) to identify h_{air} and T_{in} , and the temperatures of points 9 and 10, to obtain h_{int} , as illustrated in Fig. 10.

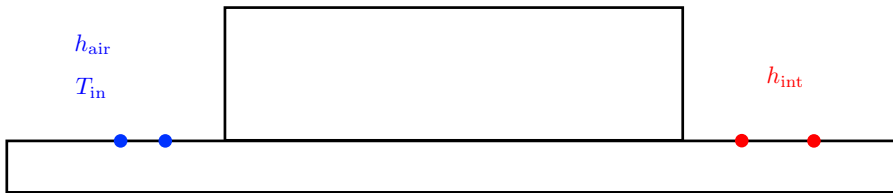


Figure 10: points used for the 2+2 points fitting test.

The results obtained in this first test, given in Table 5, show the values obtained for the error Functional, $F=74.2$ K², for the error standard deviation, $\sigma=2.72$ K.

The main advantage of the new proposed fitting methodology is the ability of allowing the identification of the required parameter set that minimizes the error functional with any number of data points, providing that it is larger than the number of parameters to identify. This is expected to provide a better, i.e. more suitable overall, result when there is enough data measured during the experimental tests. The parameter values

Table 5: Results obtained on the 2+2 points fitting test.

parameter	value
h_{int}	903.21
h_{air}	36.374
T_{in}	498.00
F	74.2
σ	2.72

obtained on the second fitting (10 points) test, where all the available temperature data points were used, are given in Table 6. As shown, by the reduction of circa 30% and 60%, respectively for F and σ , when compared with the ones of the previous fit, this approach provided better results.

Table 6: Results obtained on the 10 points fitting test.

parameter	value
h_{int}	891.40
h_{air}	32.920
T_{in}	495.29
F	50.2
σ	2.24

Additional insights of both fitting procedures can be provided by the analysis of the temperature errors obtained after the fitting procedure, shown in Table 7. On the case of the 2+2 points fitting, since on the initial step just two points are used (points 7 and 8, *cf.* Figs 10 and 6), a perfect fit is obtained at those points, with null temperature errors. Moreover, the temperature errors obtained for the 2+2 points fitting at points 9 and 10 is also lower than the ones obtained for the 10 points counterpart. This is again a consequence of the local incidence of the 2+2 point fitting procedure. The main advantages of the 10 point fitting is clear when temperature errors on the remaining points (points 1-6) are analyzed. Since the 10 points fitting procedure considers simultaneously all the measured points the temperature errors obtained at points 1-6 is lower, especially in point 3, thus providing an overall best performance.

The results obtained in this section clearly evidence the advantages of using the proposed approach with the propotype system developed for that purpose, to obtain the value of the heat transfer coefficients

7. Conclusion

In this work a novel fitting methodology to identify some unknown heat transfer coefficients of the thermoplastic profile extrusioncalibration stage, namely the interface polymer-calibrator and the air convection, was proposed. The fitting procedure employs experimental data collected with a previously developed experimental prototype system [1]. The novel methodology required the development of a modeling code for the heat transfer process, which involves discontinuous temperature and velocity fields and discontinuous materials properties. For this purpose a new second-order finite volume

Table 7: Test with h_{int} , h_{air} and T_{in} with 10 points.

point	exp. temp. [K]	2+2 points		10 points	
		mum. temp. [K]	diff. [K]	num. temp. [K]	diff. [K]
1	477.31	480.01	+2.70	476.67	-0.64
2	468.87	469.83	+0.96	469.01	+0.14
3	441.81	432.50	-9.30	437.89	-3.92
4	362.40	363.47	+1.07	363.74	+1.34
5	342.02	345.67	+3.65	345.38	+3.36
6	331.14	331.19	+0.05	331.34	+0.20
7	463.98	463.98	0.00	464.55	+0.57
8	455.32	455.32	0.00	457.89	+2.57
9	329.97	329.46	-0.51	326.31	-3.66
10	331.29	331.84	0.55	330.32	-0.97

method scheme was implemented. It is based in a cell-to-vertex reconstruction, being the vertex values computed via linear combinations of the closest cell values, where the coefficients are determined by a functional minimization. For the heat transfer coefficient identification (fitting) phase some alternative methodologies were assessed, being the Gauss-Newton method the one that showed be best efficiency in terms of calculation time and stability. Finally, the proposed methodology was tested with experimental data, which was also used to compare its performance with the one of the previous employed approach. The results obtained evidenced clearly the advantages of the newly proposed procedure.

Acknowledgements

This research was financed by FEDER Funds through Programa Operacional Factores de Competitividade — COMPETE and by Portuguese Funds through FCT — Fundação para a Ciência e a Tecnologia, within the Projects PEst-OE/MAT/UI0013/2014, PTDC/MAT/121185/2010, and UID/CTM/50025/2013. The second author was also financed by project FCT-ANR/MAT-NAN/0122/2012.

References

- [1] O.S. Carneiro, J.M. Nóbrega, A.R. Mota, C. Silva, Prototype and methodology for the characterization of the polymer-calibrator interface heat transfer coefficient, *Polymer Testing*, 32 (6) (2013) 1154–1161.
- [2] F. Marques, S. Clain, G.J. Machado, B. Martins, O.S. Carneiro, J.M. Nóbrega, A New Energy Conservation Scheme for the Numeric Study of the Heat Transfer in Profile Extrusion Calibration, submitted (preprint available in <https://hal.archives-ouvertes.fr/hal-01176796>).
- [3] C. Rauwendaal, *Polymer Extrusion 5E*, Hanser (2014).
- [4] T. Sastrohartono, Y. Jaluria, M. Essegheir, V. Sernas, A numerical and experimental study of the three-dimensional transport in the channel of an extruder for polymeric materials, *Int. J. Heat Mass Transfer*, 36 (1995) 1957–1973.
- [5] E. Mitsoulis, J. Vlachopoulos, F. A. Mirza, Finite element analysis of flow through dies and extruders channels, *SPE ANTEC Tech. Papers*, 30.53-58 (1984).
- [6] M. Gupta, T. Kown, Y. Jaluria, Multivariant finite element for the three-dimensional simulation of viscous incompressible flows, *Int. J. Numer. Meth. Fluids*, 14 (1992) 557–585.

- [7] Y. Yu, X. Luo, Estimation of heat transfer coefficients and heat flux on the billet surface by an integrated approach, *Int. J. Heat Mass Transfer*, 90 (2015) 645–653.
- [8] M.V. Murashov, S.D. Panin, Numerical modelling of contact heat transfer problem with work hardened rough surfaces, *Int. J. Heat Mass Transfer*, 90 (2015) 72–80.
- [9] H. Versteeg, W. Malalasekera, *An Introduction to Computational Fluid Dynamics: The Finite Volume Method 2E*, Pearson, Prentice Hall (2007).
- [10] C.-L. Xiao, H.-X. Huang, Optimal design of heating system for rapid thermal cycling mold using particle swarm optimization and finite element method, *Appl. Therm. Eng.*, 64 (2014) 462–470.
- [11] A. Agazzi, V. Sobotka, R. LeGoff, Y. Jarny, Optimal cooling design in injection moulding process — A new approach based on morphological surfaces, *Appl. Therm. Eng.*, 52 (2013) 170–178.
- [12] S.-C. Xue, G.W. Barton, Implementation of boundary conditions and global mass conservation in pressure-based finite volume method on unstructured grids for fluid flow and heat transfer simulations, *Int. J. Heat Mass Transfer*, 55 (2012) 5233–5243.
- [13] E.O. Reséndiz-Flores, I.D. García-Calvillo, Application of the finite pointset method to non-stationary heat conduction problems, *Int. J. Heat Mass Transfer*, 71 (2014) 720–723.
- [14] E.O. Reséndiz-Flores, F.R. Saucedo-Zendojo, Two-dimensional numerical simulation of heat transfer with moving heat source in welding using the finite pointset method, *Int. J. Heat Mass Transfer*, 90 (2015) 239–245.
- [15] W. Uffrecht, B. Heinschke, A. Günther, V. Caspary, S. Odenbach, Measurement of heat transfer coefficients at up to 25,500 g — A sensor test at a rotating free disk with complex telemetric instrumentation, *Int. J. Therm. Sci.*, 96 (2015) 331–344.
- [16] R. Costa, S. Clain, G.J. Machado, New cell-vertex reconstruction for finite volume scheme: Application to the convection-diffusion-reaction equation, *Computers and Mathematics with Applications*, 68 (2014) 1229–1249.
- [17] R. Costa, S. Clain, G.J. Machado, Finite Volume Scheme Based on Cell-Vertex Reconstructions for Anisotropic Diffusion Problems with Discontinuous Coefficients, 14th International Conference in Computational Science and Its Applications — ICCSA 2014, *Lecture Notes in Computer Science*, 8579 (2014) 87–102.
- [18] K. Levenberg, A Method for the Solution of Certain Problems in Least Squares, *Quart. Appl. Math.*, 2 (1944) 164–168.
- [19] D. Marquardt, An Algorithm for Least-Squares Estimation of Nonlinear Parameters, *SIAM J. Appl. Math.*, 11 (1963) 431–441.
- [20] H.B. Nielson, Damping Parameter In Marquardt’s Method, Technical Report IMM-REP-1999-05, Dept. of Mathematical Modeling, Technical University Denmark.